Dielectric Relaxation Studies of Segmented Polyesters

Amnuey Lilaonitkul and Stuart L. Cooper*

Department of Chemical Engineering, University of Wisconsin, Madison, Wisconsin 53706.
Received June 11, 1979

ABSTRACT: The dielectric properties of a series of poly(tetramethylene oxide)–poly(tetramethylene terephthalate) block copolymers, containing 34–84 wt % hard segment, and the poly(tetramethylene terephthalate) homopolymer have been investigated. The influence of sample composition on the various relaxation mechanisms identified suggests a two-phase structure for these segmented copolymers. Sample morphology may be described in terms of a crystalline phase of polyester segments accompanied by an amorphous phase consisting of a compatible mixture of the polyether soft segments and uncrystallized polyester units. Low-frequency dielectric measurements at frequencies from 10^{-4} to 10 Hz have been accomplished using a newly designed apparatus employing a direct ac driving signal. The relaxation spectra in the low-frequency range is interpreted in terms of Maxwell–Wagner–Sillars interfacial polarization. Analysis of the relaxation associated with interfacial polarization suggests a morphology of amorphous component ellipsoids embedded in a crystalline matrix. This model is consistent with the spherulitic texture that these materials are known to possess.

The recently developed segmented polyether–ester copolymers[1-6] are thermoplastic elastomers which exhibit the high elongation characteristic of elastomers coupled with the properties of plastics such as high modulus and strength. They also possess the ability to be processed by conventional thermoplastic processing technology. It is understood that their unusual properties result from microphase separation of the hard polyester blocks into crystalline domains, which act as physical cross-links. The amorphous elastomeric phase on the other hand consists of a mixture of soft polyether blocks and uncrystallized polyester hard segments. This two-phase semicrystalline morphology has been proposed[4,7-11] based on the results of extensive investigation using electron microscopy, small- and wide-angle X-ray scattering, small-angle light scattering, rheo-optical studies, thermal analysis, and dynamic mechanical measurements.

Since both structural units in segmented polyesters are composed of relatively polar moieties, a study of the dielectric relaxation of these materials should reveal the molecular motions characteristic of each phase. To date, modest attention has been given to the study of dipolar relaxation in block copolymer systems. Even less attention has been given to the application of dielectric methods to probe microphase morphology by studying the low-frequency process of interfacial polarization. An exception to is the recent work of North[12,13] on styrene–diene block polymers and segmented polyesters. The latter system is similar to the polymer system described in this study.

Dielectric relaxation occurs when an electric field is applied to a sample and observable polarization connected to the motion of charge carriers takes place. Within the audio frequency range, only the dipolar orientation and interfacial polarization processes are time dependent.[14,15] Interfacial polarization takes place in heterophase systems where there are boundaries between the components resulting from the difference in the permittivity and conductivity of each phase. This process termed Maxwell–Wagner–Sillars polarization[16,17] generally leads to a large dielectric dispersion which bears a direct relation to the sample morphology. Unfortunately, the process occurs at rather low relaxation frequencies, which are beyond most conventional dielectric measuring apparatus. To obtain this ultralow-frequency (ULF) information, one must typically use either a dc transient method[18,19] or a conventional ac bridge circuit employing operational amplifiers.[20-23] It is generally acknowledged that quantitative data are difficult and time consuming to obtain from the dc transient technique, while the ac bridge methods are practically limited to about 10^{-2} Hz as a lower limit of test frequency.

In this contribution, a newly developed apparatus for measuring ULF dielectric properties is described. This system requires no balancing procedure and is suitable for dielectric data acquisition down to, and in principle below, 10^{-4} Hz. The ULF experiment is accomplished within a reasonable time scale since system transients are eliminated. By combining this technique with conventional bridge methods, the dielectric behavior of segmented polyester copolymers at frequencies ranging from 10^{-4} to 10^5 Hz has been studied. Analysis of the ULF dielectric response of the system was made by comparison of the data with the various Maxwell–Wagner–Sillars models describing interfacial polarization.

Experimental Section

A. Materials and Methods. The polymers studied were formed by melt transesterification of 1,4-butanediol, dimethyl terephthalate, and poly(tetramethylene ether glycol) (PTMEG). The molecular weight of the PTMEG sequence is approximately 1000. The resultant segmented polymer shown below consists of randomly jointed PTMO soft segments and sequences of tetramethylene terephthalate (4GT) hard segments.

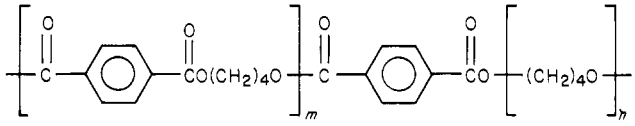

hard segment soft segment

The overall molecular weight of the copolymers was approximately 25000–30000. A series of four segmented polyether–esters consisting of 34 to 84% by weight of poly(tetramethylene terephthalate) (PTMT) hard segment and the PTMT homopolymer were studied. Material characteristics are shown in Table I.

Samples were prepared by compression molding at temperatures of about 25 °C above the highest melting transition of each sample at a pressure of approximately 1500 psi. Samples for low frequency dielectric study were purified prior to compression molding by precipitation from trichloroethane, using methanol as a nonsolvent. This was followed by vacuum drying at 100 °C for 3 days. Samples are identified by the weight percent of 4GT such that H34 indicates a copolymer containing 34 wt % 4GT units. Dielectric measurements at frequencies from 10^2 to 10^5 Hz were made using a Krohn-Hite Model 4100R oscillator, a General Radio 1615A capacitance bridge, and a Princeton Applied Research lock-in amplifier Model 129A for null detection. The conductance range of the GR bridge has been extended to 1 $\mu\Omega^{-1}$ by connecting a high precision resistor of 10^6 Ω to the external standard terminals of the bridge. Samples of about 55 mil thickness were placed in a three-terminal condensor, Balsbaugh

0024-9297/79/2212-1146$01.00/0

Table I
Sample Characterization

	H34	H49	H63	H84	PTMT
wt % of PTMT	34	49	63	84	100
av PTMT block length	2.7	4.8	8.1	24.3	
T_g, °C					
as received	−68	−59	−51	−9	+50
purified	−68				
purified and annealed	−68	−65	−59		
T_m, °C	163	189	200	214	222
% crystallinity					
as received	11.5	22.9	33.3	42.8	49.1
purified	13.0		36.0		
purified and annealed	18.5	28.2	36.0		
crystalline vol fraction, v_c					
as received	0.086	0.181	0.276	0.382	0.464
purified	0.098		0.299		
purified and annealed	0.140	0.224	0.299		

cell Model LD-3. This parallel plate guarded cell exhibits a temperature-dependent air capacitance which has been corrected for in the data analysis. Data were also corrected for errors introduced by the nonlinear relation between the conductance and resistance of the bridge as suggested by the GR 1615A instructional manual. Temperature was controlled using a Ransco cryogenic test chamber, Model SD 14-1.

Dielectric experiments at frequencies from 10^{-4} to 10 Hz were performed at 21 °C, using the newly designed ULF dielectric measuring system. The sinusoidal driving signal was provided by a Hewlett Packard function generator, Model 3310B, at frequencies ranging from 10^{-4} to 10 Hz. This driving signal was smoothed by a Rockland Model 452 filter. The sample response from the output of the current to voltage converter and the filtered driving sine wave were monitored simultaneously as a function of time by a Gould multichannel recorder, Model Brush 440. Frequencies of the driving signals were determined from the recorded period of the sine wave and the chart speed of the recorder. Measurements of the amplitude and the phase relationships of the two signals provide the necessary information for the computation of C_x, R_x, ϵ', and tan δ of the sample. These terms represent the capacitance, resistance, dielectric constant, and loss tangent of the specimen. Further detail on this apparatus is provided in the following section.

Thermograms of samples over the temperature range −150 to +240 °C were recorded by a Perkin-Elmer DSC II at a heating rate of 20 °C/min under a He purge. Percent crystallinity for partially crystalline samples was determined from the melting endotherm at a heating rate of 10 °C/min with a N_2 purge. Sample weights were 15 ± 3 mg.

B. ULF Dielectric Test Assembly. 1. Theory of Operation. An ultralow-frequency dielectric measuring system has been developed whereupon application of a low-frequency sinusoidal driving voltage to a test specimen the current response is simultaneously monitored. Two major difficulties are expected in this ULF experiment. The first is the possibility of an electrical transient associated with some time constant of the circuit assembly. The second involves the recording of a very small current resulting from the extremely high impedance of the sample at low frequencies. The latter can be remedied by decreasing the thickness to area ratio of the sample and using an electrometer-grade amplifier as a buffer for the detector.

The transient characteristics of the system may be studied based on the analysis of the simple circuit shown in Figure 1. By applying an excitation function of $V = V_0 \sin(\omega t + \theta)$, we can express the current response as

$$i(t) = V_0 C_x\{\sin\theta\delta(t) + (\omega_x \cos\theta - \omega \sin\theta) \sin\omega t + (\omega \cos\theta + \omega_x \sin\theta) \cos\omega t\} \quad (1)$$

where $\omega_x = 1/R_xC_x$, $\omega = 2\pi f$ (the angular frequency), and $\delta(t)$ is the Dirac delta function. Obviously this circuit shows no transient in the current expression. Shortly after the application of the driving signal, the first term of eq 1 is eliminated. In a more general form, the time-dependent current can be written as

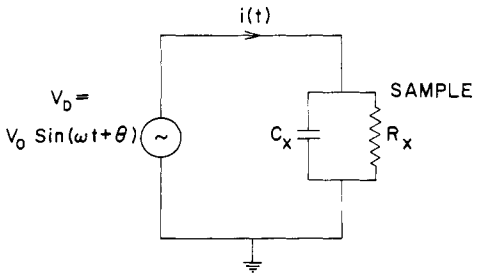

Figure 1. Basic circuit for ULF dielectric measurements.

$$i(t) = I_0 \sin(\omega t + \phi + \theta) \quad (2)$$

where ϕ is the relative phase angle between the stimulus and the response. Comparing eq 1 and 2, one obtains

$$\phi = \tan^{-1}(\omega R_x C_x) \quad (3)$$

and

$$I_0 = \frac{V_0}{R_x}[1 + \omega^2 R_x^2 C_x^2]^{1/2} \quad (4)$$

Knowing I_0 and ϕ, we can compute the values of R_x and C_x of the sample to provide the necessary information for determining the dielectric properties of the sample.

$$\epsilon' = \frac{C_x}{C_0} = \frac{I_0}{V_0 C_0} \frac{\cos\delta}{2\pi f} \quad (5)$$

$$\tan\delta = \frac{\epsilon''}{\epsilon'} = \cot\phi = (\omega R_x C_x)^{-1} \quad (6)$$

In general, the resistance of the sample, R_x, at any instant is considered to consist of two components, namely, a conduction term R_0 and a nonconduction or relaxation term R_1, connected in parallel such that $(R_x)^{-1} = (R_0)^{-1} + (R_1)^{-1}$. By substitution of the R_x term in eq 6, the loss tangent becomes

$$\tan\delta = (\omega R_0 C_x)^{-1} + (\omega R_1 C_x)^{-1} = \tan\delta_0 + \tan\delta_1 \quad (7)$$

where tan δ_0 and tan δ_1 are the loss due to dc conduction and relaxation, respectively. In order to obtain the contribution from the dc conduction, we must either measure the dc conductance of the sample directly or identify a region of the tan δ spectrum where the loss tangent varies inversely with frequency. According to eq 7, if a log–log plot of tan δ vs. frequency yields a straight line with a slope of −1, the frequency-dependent term due to R_1 will be absent. By knowing C_x, one can obtain R_0 through the tan δ expression,

$$R_0 = (2\pi f C_x \tan\delta)^{-1} \quad (8)$$

where in this case tan δ = tan δ_0. Subsequently, tan δ_0 at any frequency can be computed, and the loss due to the relaxation process, tan δ_1, can be obtained through eq 7.

2. Circuit Description. The complete circuit diagram of the ULF measuring system is illustrated in Figure 2.

The major component of the system is the precision FET-input electrometer grade operational amplifier (OA) which serves as an inverting current to voltage converter. The Analog Device AD 515 op-amp is used in our circuit construction because it has an input impedance of 1.6 pF//10^{13} Ω in the differential mode and 0.8 pF//10^{15} Ω in the common mode. The input bias current of this OA is 75 × 10^{-15} A maximum, providing that the input lines to the OA have been properly guarded. Special care should be exercised in the PC board layout and construction so that the electrical path of the signal source to the measuring device is as short as possible in order to minimize current leakage paths, noise pickup, and capacitive loading. A high-quality glass-encapsulated resistor, Victoreen RX-1 Hi-Meg, with 1% accuracy was used as the feedback resistor, R_{FI}. This resistor determined the gain of the current to voltage converter. An E_0 of −1 μV/pA or −1 mV/pA can be obtained when R_{FI} is 10^6 or 10^9 Ω, respectively. Glass-

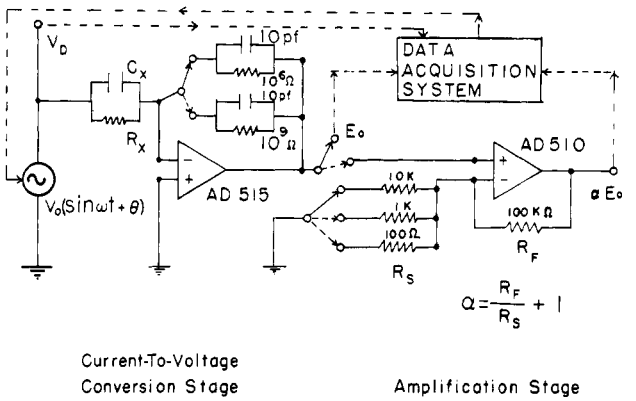

Figure 2. Circuit diagram for the ULF current detection.

encapsulated capacitors in parallel to R_{FI} are recommended to stabilize the circuit especially at very low signal levels. The signal from the high-impedance source is carried on the line connected to the inverting input of the OA and shielded by the ground line. The output voltage E_0 of the AD 515 op-amp can be further amplified by the second stage IC op-amp, AD 510, which is connected in the noninverting configuration. Finally, the additional constraints in performing experiments are that rigid and low-noise-shielded coaxial cable must be used for noise reduction.

The frequency range of the present apparatus is limited by two major factors. The low-frequency limit is set by the range of the signal generator used, whereas the highest frequency attainable is limited by the current detection system. The latter is directly related to the performance and frequency response of the OA which is used as the current to voltage converter. In addition, phase correction may be necessary if the experiment is carried out at frequencies beyond the operational limits as determined by the feedback resistor (R_{FI}), feedback capacitors, and the input capacitance of the OA.

Results and Discussion

A. Thermal Analysis. DSC thermograms of materials used in this study reveal an amorphous-phase glass transition and a crystalline-phase melting endotherm. Values of T_g and T_m for the as received, purified, and annealed samples are summarized in Table I. The fact that T_g shows a progressive shift with increasing PTMT content suggests that uncrystallized hard segments form a compatible amorphous phase with the polyether component.[8-10] It has been previously shown[9] that the T_g behavior of these segmented copolyesters can be accurately modeled by the Gordon–Taylor equation,[24] provided that the PTMT crystalline phase was not included in the calculation.

Figure 3 shows the DSC thermograms of samples used in the ULF dielectric experiment. These curves were used to determine the degree of crystallinity of the materials. Samples designated by codes terminating by the letter A were annealed at 125 °C under vacuum for 24 h. The heat of fusion, ΔH_f, for each sample was determined from the area under the melting endotherm. The degree of crystallinity was evaluated by comparison of the endotherm area with the value of ΔH_f for the PTMT homopolymer of 31.4 kJ/mol, assuming 100% crystallinity.[25] An increase in hard segment content raises the degree of crystallinity of the sample. Annealing also results in an increased crystallinity, the extent of which decreases as the hard segment concentration increases. A pronounced change in the crystalline character of sample H34 results from annealing. The annealed sample H34A shows a much narrower distribution of crystal size and a large increase in crystallinity. This may be attributed to the fact that annealing is a process involving melting and recrystallization of unstable small crystals as well as secondary crystallization. The annealing condition used is close to the melting point of sample H34 and leads to a substantial reorganization of the crystalline phase.

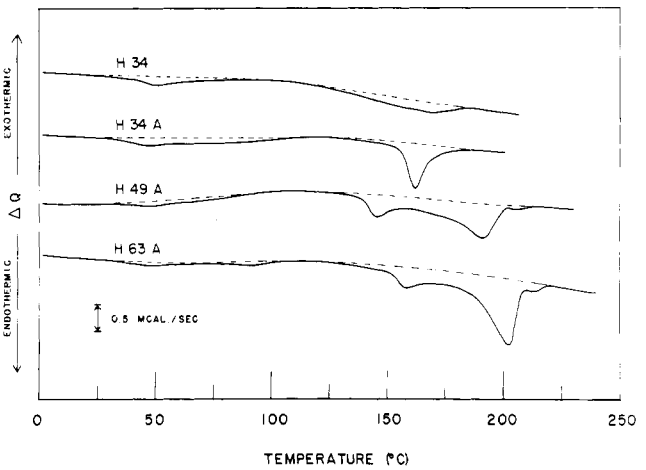

Figure 3. DSC thermograms of samples H34, H34A, H49A, and H63A used for the degree of crystallinity determination.

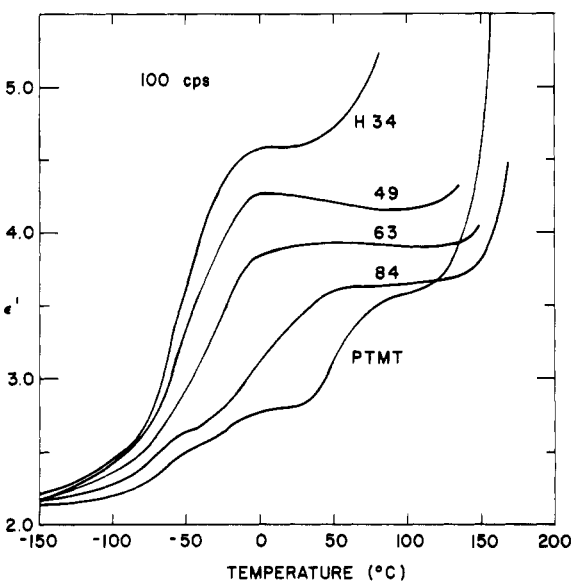

Figure 4. Dielectric constant as a function of temperature at 100 Hz for PTMEG/4GT copolymers.

The crystalline volume fraction for each sample was estimated using the relation

$$v_c = (\rho - \rho_A)/(\rho_c - \rho_A) \quad (9)$$

where ρ is the bulk sample density, ρ_c is the density of the pure PTMT crystalline phase, 1.433 g/cm^3,[26] and ρ_A is the amorphous density which is assumed to vary with composition. Assuming linear additivity of specific volumes, we estimated ρ_A by the random copolymer equation

$$1/\rho_A = W_1/\rho_1 + W_2/\rho_2 \quad (10)$$

In the case of ρ_A determination, ρ_1 and ρ_2 are 0.98 and 1.286 g/cm^3 for amorphous poly(tetramethylene oxide)[27] and PTMT,[28] respectively. The weight fractions were then normalized to exclude the crystalline PTMT hard component. Values of v_c are shown in Table I.

B. High-Frequency Dielectric Properties. The dielectric behavior of polyether–ester copolymers as well as the PTMT homopolymer as a function of temperature at 100 Hz are displayed in Figures 4 and 5. The dielectric permittivity ϵ' spectra shown in Figure 4 have been corrected for errors introduced by the temperature dependence of the parallel plate guarded cell. The uncorrected

Table II
Dielectric Properties of PTMEG/4GT and PTMT Polymers

	γ transition			β transition		
	T_{max}, °C[a]	ϵ_{max}''[b]	ΔH_a[c]	T_{max}, °C[a]	ϵ_{max}''[b]	ΔH_a[c]
H34	−96	0.044	9.6	−42	0.136	36.8
H49	−98	0.0373	9.9	−35	0.105	43.4
H49W	−100	0.0362	8.5	−38	0.118	48.8
H63	−94	0.0302	10.0	−23	0.0732	51.6
H63A	−97	0.0298	10.3	−29	0.072	42.4
H84	−65	0.0242	16.1	+27	0.052	59.4
PTMT	−45	0.0281	14.9	65	0.0656	63.3
PTMT-W	−45	0.0337	15.3	62	0.0592	62.6
PTMT-A	−45	0.0236	15.1	67	0.044	69.6

[a] ϵ_{max}'' peak at 1K Hz. [b] Measured at 1K Hz. [c] Unit in kcal/mol.

raw data indicated an increase of the apparent dielectric constant with decreasing temperature at temperatures below −100 °C (prior to the major transition). Similar results have been reported by Ashcraft and Boyd[29] in their dielectric study of oxidized and chlorinated polyethylene in which they attributed the observation to both the densification of the sample and the declining plate separation of the parallel plate guarded cell.

The effect of the 4GT hard segment content on the dielectric constant of these copolymers is clearly illustrated in Figure 4. The sample dielectric strength ($\epsilon_R - \epsilon_U$) varies from about 2.4 to 1.5 in going from sample H33 to H84. Increasing the 4GT composition tends to shift the major transition to higher temperature and broadens the transition temperature range. In samples containing high 4GT concentration, e.g., H84, an additional secondary relaxation appears at about −70 °C. This relaxation also appears in the PTMT homopolymer. At very high temperatures, all samples exhibit an abrupt increase in the apparent dielectric constant.

Figure 5 shows the dielectric loss tangent spectrum at 100 Hz for these materials where several molecular relaxation processes are observed. The relatively broad peak appearing at very low temperatures (approximately −115 °C at 100 Hz) is denoted as the γ transition. The intensity of the γ transition peak decreases as the 4GT content increases. The γ peak becomes highly asymmetric in sample H84, characteristic of a multiple-relaxation process. Carefully resolving the peak indicates that two relaxation processes are involved, namely, the γ transition as observed in samples H34 through H63 and the γ transition observed in the PTMT hard segment homopolymer. The next transition in these copolymers which appears at higher temperature is termed the β relaxation. Increasing the 4GT concentration causes the β peak to broaden, its magnitude to decrease, and its position to shift to higher temperature. At high 4GT concentration the shape of the β peak is also asymmetric, as it is broader on the high-temperature side of the peak. At very high temperatures, the tan δ curve rises sharply, while including an apparent shoulder. The position of this shoulder is composition dependent, and the molecular relaxation associated with this process is called the α transition, in accord with the α peak observed in the dynamic mechanical results previously reported.[9] At the highest temperatures are some polarizations, denoted as the η process, which are not directly related to the melting of the crystalline phase since the transition occurs at a temperature far below the melting point of the sample. This huge loss tangent has not been observed in the dynamic mechanical testing of the same polymers. It is believed that the molecular mechanisms involved in the η process may be attributed to the dc conduction of the bulk sample and Maxwell–Wagner–Sillars polarization at the amorphous–crystalline interfacial regions.

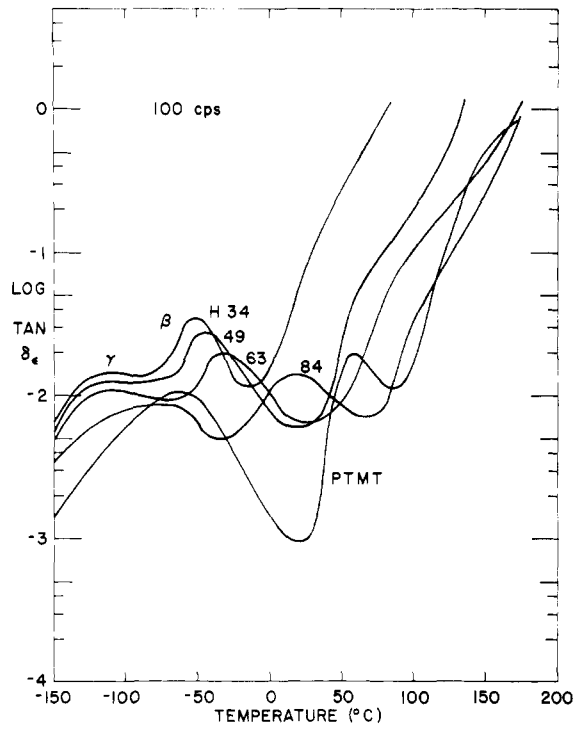

Figure 5. Dielectric dissipation factor as a function of temperature at 100 Hz for PTMEG/4GT copolymers.

In order to elucidate the molecular mechanisms associated with the γ and β transitions, dielectric measurements were carried out at various frequencies. The resultant ϵ' and ϵ'' curves plotted against temperature at 100, 1K, and 10K Hz of sample H63 are shown in Figure 6. Increasing the frequency tends to move the ϵ' and ϵ'' spectrum laterally to the right (higher temperatures), as predicted by the time–temperature superposition principle. Figure 7 shows plots of the logarithm of the loss maximum frequency (f_{max}) versus reciprocal absolute temperature ($1/T_{max}$) for both the γ and β relaxations of these copolymers and the PTMT homopolymer. Within the range of frequencies studied, the relation between log f_{max} and $1/T$ appears to be linear for both processes in all samples. The corresponding activation energy ΔH_a of the γ and β relaxations for these materials is summarized in Table II. The activation energies associated with the γ relaxation for samples H34 to H63 are about 9.6 to 10 kcal/mol, which is in good agreement with the results of the dielectric study of poly(tetramethylene oxide) (PTMO) by Wetton and Williams,[30] who reported an activation energy of 9.7 kcal/mol for the process. Thus the γ transition of these

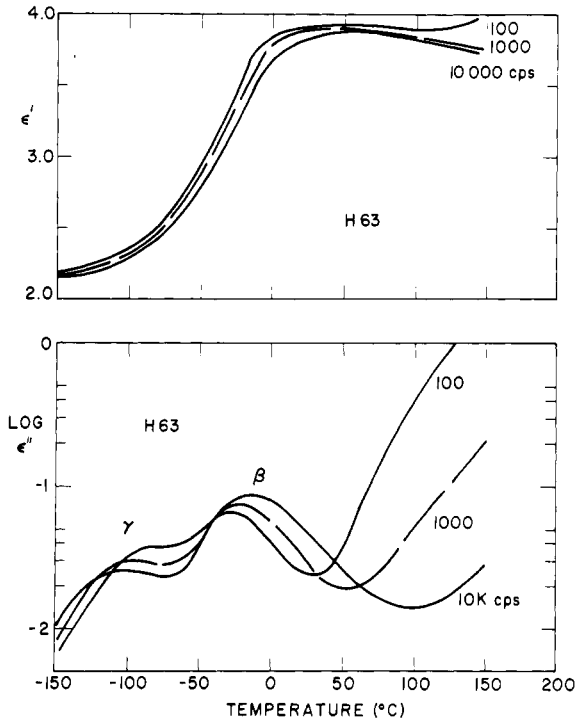

Figure 6. Dielectric constant and loss factor as a function of temperature at 100, 1K, and 10K Hz of sample H63.

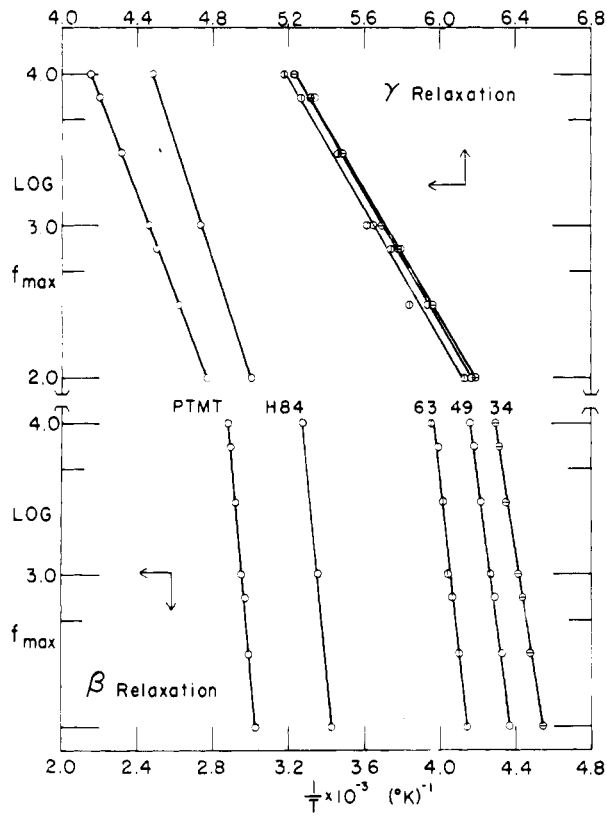

Figure 7. Plots of log f_{max} vs. $1/T$ of the γ and β processes for PTMEG/4GT copolymers and PTMT homopolymer.

copolymers was assigned to local mode molecular motions associated with the soft segments. However, the dielectric γ process could not be due to the independent motions of the $(CH_2)_4$ units, since in order to be dielectrically active, motion of the ether group must occur. It is thus believed that the γ process is due to the local mode motions of the soft segment $-(CH_2)_4O-$ units in accord with the theory of Yamafuji and Ishida.[14] As the 4GT composition becomes very high, i.e., in sample H84 the amorphous phase consists of 70% uncrystallized 4GT hard segments, the γ process of the noncrystalline 4GT segments predominates. Extensive studies of poly(ethylene terephthalate) (PET) homopolymer have been previously done, and the dielectric and dynamic mechanical properties of this polyester have been reviewed by McCrum et al.[14] They concluded that the γ transition of PET contained three distinct processes, including hindered rotation of CH_2 groups at −165 °C observed only in the mechanical study and motions of the dipolar COO units at −105 and −70 °C. The latter two peaks were associated respectively with the gauche and trans conformation of the polymer chain. It is these latter processes which dominate the overall γ transition. The reported apparent activation energy was 12.9 kcal/mol for the dielectric γ relaxation in dry and wet, amorphous, and crystalline PET. In this work, the γ process of pure PTMT was found at −65 °C, as seen in Figure 5, with an activation energy of about 15 kcal/mol (Table II). Due to the asymmetric shape of the peak, it is concluded that the process involves the molecular motions of the COO units of different conformations. A PTMT sample annealed at 200 °C for 4 h showed a decrease in ϵ_{max}'' (Table II) which suggested that the COO motions are in the noncrystalline regions. Consequently, there are two relaxation processes for the γ transition in sample H84. The lower temperature process involves the local mode motion of the ether group in the soft segments, while the higher temperature process is associated with the local motion of COO units of the uncrystallized hard segments.

The dielectric behavior of the β transition of the PTMEG/4GT copolymers was consistent with observations of their dynamic mechanical properties.[9] The activation energy of this relaxation process varies progressively from 36.8 to 59.4 kcal/mol as the hard segment composition increases from 34 to 84 wt %, respectively. The magnitudes of the activation energy for the β transition are on the order of those found for the primary dispersion (T_g) of amorphous polymers. The PTMT homopolymer exhibits an activation energy of 63.3 kcal/mol for the β process, as shown in Table II, while the reported value of poly(tetramethylene oxide) homopolymer is about 37 kcal/mol.[31] The dielectric results, therefore, confirm that the β relaxation was due to the large-scale motion (T_g) of the noncrystalline phase of the material which is comprised of a mixture of the PTMEG soft segments and uncrystallized 4GT hard segments. At low hard-segment content this amorphous phase was richer in soft segments (low T_g and ΔH_a comparable to those of pure PTMO), while the opposite was true at high 4GT concentration. Although the two components of the amorphous phase may not be completely soluble in each other, the mixture becomes more compatible as the 4GT content decreases, indicated by the narrower width of the absorption peak. The broadening of the β peak as a function of 4GT composition may be attributed to a broadening of the distribution of relaxation times associated with micro-Brownian motion of the amorphous phase. The asymmetry of the peak is due to the restriction of these motions by the crystalline phase of the sample. The latter has been observed in many semicrystalline polymers,[14] where an increase in the degree of crystallinity results in an asymmetric broadening of the absorption peak on the high-temperature (isochronal experiment) or low-frequency (isothermal experiment) side.

The effects of annealing and absorbed water on the dielectric properties of these samples have also been investigated. The results of control and pretreated samples are compared for samples H49 and H63 in Figure 8. For

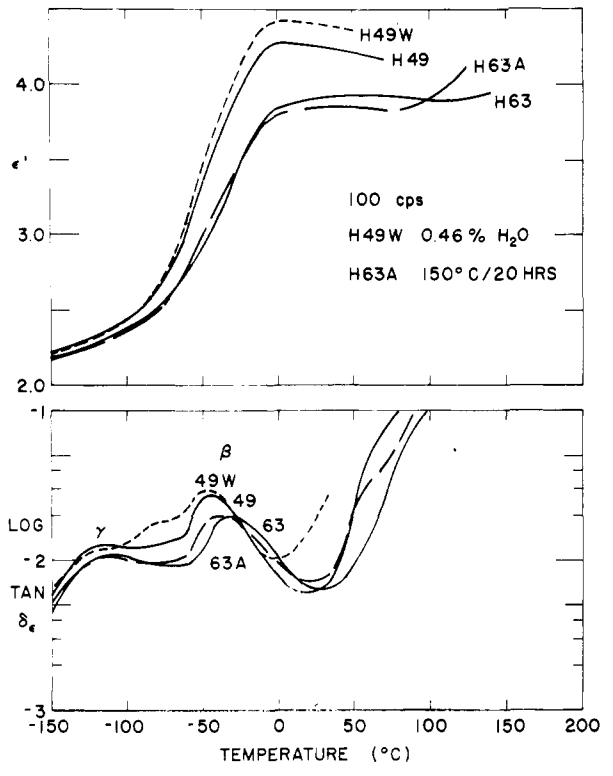

Figure 8. Effects of annealing and absorption of water on the dielectric properties of PTMEG/4GT copolymers.

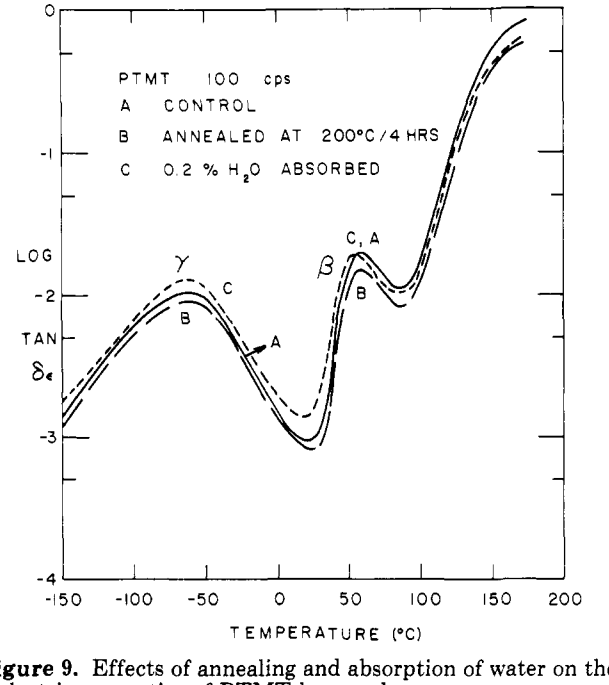

Figure 9. Effects of annealing and absorption of water on the dielectric properties of PTMT homopolymer.

the β transition both treatments had negligible effect on ϵ_U (the low-temperature limit ϵ'), while some pronounced differences were observed in ϵ_R (the high-temperature limit of ϵ'). Samples containing an appreciable amount of water showed an increase in ϵ' through the β transition, and a slight decrease in intensity and peak temperature of the γ peak. In addition the β peak had an increased amplitude and was shifted to a lower temperature. Finally, an additional peak coincident with the γ peak of the PTMT homopolymer appeared in the wet sample. Study of the apparent activation energy of both γ and β transitions showed an increase in the β and a decrease in the γ activation energies. These particular features can be explained if one imagines that water molecules act mainly as a mechanical amplifier of a low-amplitude motion which is intrinsic to the backbone chain.[32] The absorbed water molecules, forming hydrogen bonds which are tightly bound to the carbonyl group of the hard segments in the amorphous phase, are regarded as short branches of the polymer chain. This results in an increase of the polarizability of the chain segment. Thus, the intensity of the dielectric relaxation associated with the local mode motions of the COO group in the hard segment increases, which leads to the observation of the relaxation peak at about −75 °C in Figure 8. These tightly bound water molecules in the amorphous phase enhance the energy barrier for the micro-Brownian motion of the mixed elastomeric phase. Consequently, an increase in the ΔH_a of the β transition is expected. The lower γ activation energy, on the other hand, may be attributed to the increase in free volume introduced by water molecules absorbed on the polymer backbone. It should be noted that no data on the activation energy of the relaxation peak of absorbed water molecules could be obtained because the peak overlapped with the β peak as the driving frequency increased.

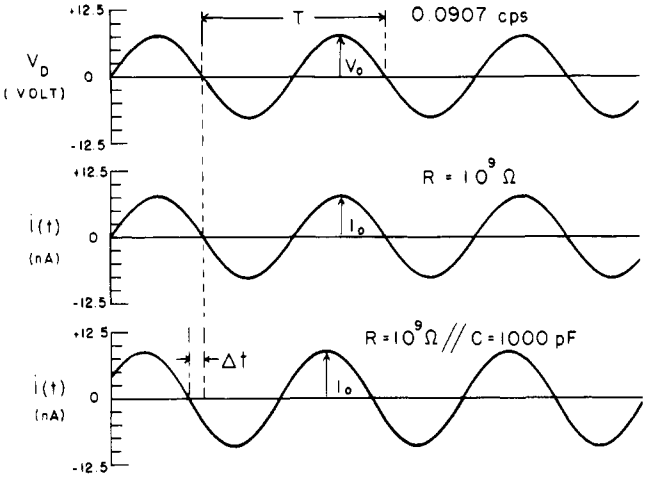

Figure 10. Experimental results obtained from the ULF measuring system on standard electrical elements at 0.1 Hz.

The dielectric results of annealed H63 shown in Figure 8 were in good agreement with previous work[9] on the dynamic mechanical properties of this sample. Annealing of the sample decreases the ϵ' plateau succeeding the β transition and shifts the β peak to lower temperature. Annealing had a negligible effect on the γ peak. The annealed sample had an activation energy of 42.4 kcal/mol for the β relaxation as compared to 51.6 kcal/mol of the control sample. The explanation here is parallel to that presented in the dynamic mechanical study which concluded that annealing results in an amorphous phase richer in the polyether segments. As a consequence, T_g and its corresponding activation energy are expected to approach those of the poly(tetramethylene oxide) homopolymer. Apparently, the restriction to the movement of polyether segments due to the increase in degree of crystallinity was outweighed by the increased mobility of the more pure amorphous phase produced as the 4GT segments leave to become attached to crystalline lamellae.

No study was carried out on the dielectric α process observed because of the difficulties in resolving the peak at high temperatures. However, the approximate position of the process and how it was affected by composition and annealing seem to confirm the conclusion drawn from the dynamic mechanical study[9] that this α process is associated with defect regions of the 4GT crystallites. The Max-

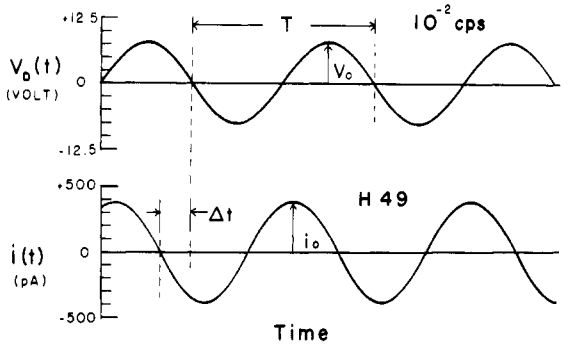

Figure 11. Current response of sample H49 at 0.01 Hz.

well–Wagner–Sillars interfacial polarization is described in more detail in the following section.

C. Low-Frequency Dielectric Behavior. 1. Function of the ULF Dielectric Test Assembly. Figure 10 illustrates the traces from the recorder of the driving sinusoidal signal and the sampled signals at a frequency of 0.0907 Hz. For illustration purpose, a unity inverter was placed at the input terminal of the recorder which carried the sampled signals in order to eliminate the phase inversion from the AD 515 amplifier. When the sample is a standard resistor of 10^9 Ω (Victoreen RX-1 Hi-Meg Resistor with 1% accuracy), the sample response is also sinusoidal, totally in phase with the exciting signal. A phase lead (Δt) of the sampled signal over the driving signal is observed when a standard air capacitor of 999.6 pF (GR 1422-CB Variable Precision Capacitor) is connected in parallel with the resistor. Theoretically, the value of the phase angle can be computed using eq 2, where in this particular case $\phi = \tan^{-1}(2\pi fRC) = \tan^{-1}(0.5697) = 0.5178$ radians where f is 0.0907 Hz. Experimentally, the phase angle can simply be expressed as

$$\phi = (\Delta t/T)2\pi \qquad (11)$$

where Δt is the phase lead or lag of the sample response in the same units as the period, T, of the driving signal. In this case, $\Delta t = 0.45$ cm while $T = 5.51$ cm, which results in a value of $\phi = 0.513$. Obviously the experimental result and the theoretically predicted value of ϕ are in good agreement (0.9% error). This is quite satisfactory, considering the errors which may be involved in the manual determination of Δt, T, and f and the uncertainty of the values of R and C used. A higher accuracy in the measurements of Δt, T, and f will be possible when a computerized data acquisition system which has been under development is in operation. Initial work indicates that resolution of 0.01° in δ should be possible routinely. With this apparatus, each of the two sinusoidal signals is sampled thousands of times during a cycle, with values being stored in the memory of a PDP 11/03 processor via 12-bit analog-to-digital converters. The stored information is operated on with integral, regressive, or more advanced techniques, in order to extract the complex dielectric constant as a function of frequency.

It should be noted that the data of the present publication have been obtained using the two-channel recorder system mentioned above. The ULF experimental result for the unannealed sample H49 as well as the driving sine wave at a frequency approximately of 10^{-2} Hz are shown in Figure 11. The sample characteristics at low frequencies are revealed by the values of I_0 and Δt observed. No changes are observed in the magnitude of I_0 and Δt over several cycles, as predicted by eq 1.

2. ULF Dielectric Relaxation of Polyether–Polyester Copolymers. Figures 12 and 13 show the dielectric

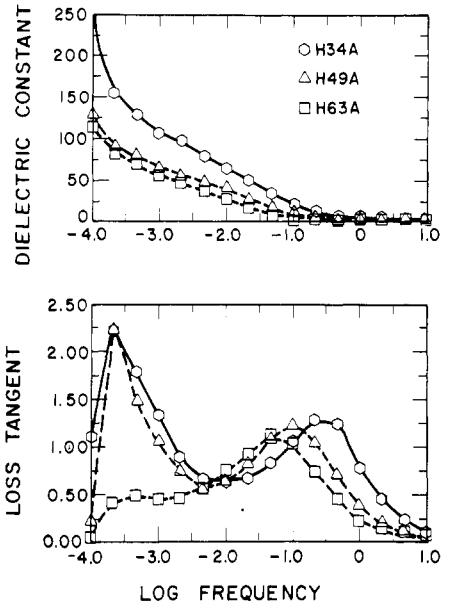

Figure 12. ULF dielectric spectra for annealed PTMEG/PTMT copolymers.

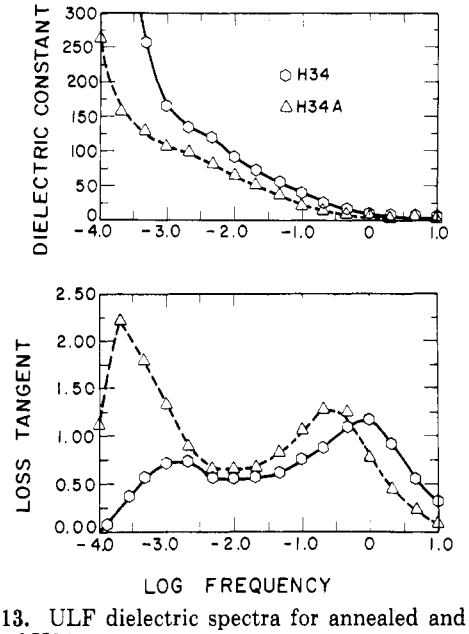

Figure 13. ULF dielectric spectra for annealed and control samples of H34.

constant, ϵ', and loss tangent, tan δ, of segmented copolyesters at frequencies from 10^{-4} to 10 Hz. All tan δ curves have been corrected for the loss associated with dc conductivity. Two low-frequency relaxation peaks are resolvable and are designated as processes I and II in order of decreasing frequency. These processes are obviously not associated with dipolar polarization of either the amorphous or crystalline phase, as indicated by the enormous dielectric dispersion observed. Presently, the exact nature of the process II relaxation which occurs at frequencies below 10^{-3} Hz is unknown. The mechanism could involve electrode polarization, charge carrier hopping between trapping sites, or interfacial polarization, all of which can cause large dielectric losses at low frequencies.[12,17,33,34] Process I, on the other hand, reveals relaxation behavior characteristic of interfacial polarization, arising from a multiphase sample morphology. The dielectric relaxation parameters of this process for the three samples investigated are summarized in Table III.

Table III
Low-Frequency Dielectric Properties of PTMEG/4GT Copolymers

sample	ϵ_∞	ϵ_s	τ_D, s
H34	5.146	130	1.2
H34A	4.777	105	3.4
H49A	4.277	52	11.2
H63A	4.046	50	18.6

Figure 12 shows the effect of sample composition on interfacial polarization behavior of these copolymers. An increase of hard segment content leads to an increase in relaxation time and a decrease in both the amplitude of the loss peak and the static dielectric permittivity. These are primarily brought about by changes in phase composition, morphology, and electrical properties of the amorphous phase as the copolymer composition changes. In addition, the purity and perfection of the PTMT crystalline domain may also play an important role in the Maxwell–Wagner–Sillars polarization of these samples. The effect of crystal perfection can be clearly seen in Figure 13, which compares the ULF dielectric spectrum of annealed and control samples of H34. Annealing of the sample leads to a longer relaxation time and an increase in both the loss amplitude and dielectric strength of the interfacial polarization process. In order to elucidate the ULF dielectric relaxation behavior of these materials, the Maxwell–Wagner–Sillars (MWS) dielectric theory of heterophase systems was applied to these segmented copolymers. It should be noted that parallel studies of similar materials, using the dc transient technique, have recently been reported by North et al.[13] However, in the latter study the dielectric dispersions determined were relatively small, and correlation between (MWS) theory and experimental results was not possible.

The various dielectric theories of heterophase systems have been recently reviewed.[12,17] The general expressions based on MWS theory which describe the relaxation behavior of a two-phase system with a dilute and randomly oriented suspension of spheroids of volume fraction v_2 dispersed phase 1 are:

$$\epsilon_\infty = \epsilon_1\left[1 + \tfrac{1}{3}v_2(\epsilon_2 - \epsilon_1)\sum_i \frac{1}{\epsilon_1 + A_i(1 - v_2)(\epsilon_2 - \epsilon_1)}\right] \quad (12)$$

$$\epsilon_s = \epsilon_1\left[1 + \tfrac{1}{3}v_2(\sigma_2 - \sigma_1)\sum_i \frac{1}{\sigma_1 + A_i(1 - v_2)(\sigma_2 - \sigma_1)}\right] + \tfrac{1}{3}v_2\sigma_1\sum_i \frac{(\sigma_1\epsilon_2 - \sigma_2\epsilon_1)}{[\sigma_1 + A_i(1 - v_2)(\sigma_2 - \sigma_1)]^2} \quad (13)$$

$$\bar{\tau} = \tfrac{1}{3}\epsilon_0\sum_i\left[\frac{\epsilon_1 + A_i(1 - v_2)(\epsilon_2 - \epsilon_1)}{\sigma_1 + A_i(1 - v_2)(\sigma_2 - \sigma_1)}\right] \quad (14)$$

and

$$\bar{\tau}_D = (\epsilon/\epsilon_s)^{1/2}\bar{\tau} \quad (15)$$

Here, ϵ_0 is the permittivity of free space (8.85×10^{-12} F/m), and ϵ, σ, and $\bar{\tau}$ have their general meanings of permittivity, conductivity, and average relaxation time, respectively. A_i is the depolarization factor along the i axis of the occluded ellipsoids,

$$A_i = \frac{abc}{2}\int_0^\infty \frac{ds}{(s + i^2)[(s + a^2)(s + b^2)(s + c^2)]^{1/2}} \quad (16)$$

for $i = a$, b, and c. Values of A_i for prolate and oblate ellipsoids at various axial ratios can be found elsewhere.[35] To apply MWS dielectric theory, values of the permittivity and conductivity of each phase must be determined independently. ϵ_c and σ_c for the pure PTMT phase were estimated as $\epsilon_c = 2.15$ (from the high frequency dielectric constant of the PTMT sample at −150 °C, which presumably contains only electronic and atomic polarization contributions) and $\sigma_c = 10^{-16}$ $(\Omega\ m)^{-1}$. The permittivity of the amorphous phase was then evaluated, using the Looyenga equation[36]

$$\epsilon = [\epsilon_1^{1/3} + v_2(\epsilon_2^{1/3} - \epsilon_1^{1/3})]^3 \quad (17)$$

which has been found to be applicable for semicrystalline polymers.[37] By substituting σ for ϵ in eq 17, the conductivity of the amorphous phase was determined. The results are summarized in Table IV.

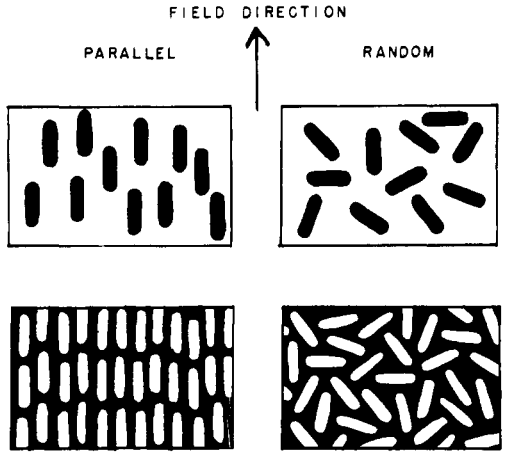

Figure 14. Idealized models of occluded spheroids oriented parallel and randomly to the field.

The theoretical dielectric relaxation parameters of the four samples at various elliptic axial ratios with a continuous matrix consisting of either the amorphous phase or the crystallite phase are compared with the experimental values in Tables V–VIII. The calculation shown was based on two different morphologies, where the long axis of the occluded ellipsoids is either parallel or randomly oriented to the electric field. A schematic model of these morphologies is shown in Figure 14. The light and dark regions represent the amorphous and crystalline phase, respectively. Obviously, the theoretical parameters are not in good agreement with the experimental results for the amorphous matrix cases. On the other hand, both ellipsoidal orientation morphologies assuming a crystalline matrix yielded calculated values comparable to the experimental results. Possibly the model of randomly oriented amorphous ellipsoids gives a better correlation in both ϵ_s and $\bar{\tau}_D$. This approach suggests a structure of randomly oriented ellipsoidal amorphous domains dis-

Table IV

sample	permittivity			conductivity, $(\Omega\ m)^{-1}$		
	ϵ (10 Hz)	ϵ_a	ϵ_c	σ	σ_a	σ_c
H34	5.146	5.581	2.15	7.86×10^{-11}	1.07×10^{-10}	10^{-16}
H34A	4.777	5.343	2.15	2.74×10^{-11}	4.31×10^{-11}	10^{-16}
H49A	4.277	5.082	2.15	5.89×10^{-12}	1.26×10^{-11}	10^{-16}
H63A	4.046	5.112	2.15	2.22×10^{-12}	6.4×10^{-12}	10^{-16}

Table V
Relaxation Parameters of Sample H34 Predicted by MWS Theory

	parallel			random		
	ϵ_∞	ϵ_s	$\bar{\tau}_D$	ϵ_∞	ϵ_s	$\bar{\tau}_D$
	Crystalline Ellipsoids in an Amorphous Matrix					
exptl results	(5.146)	(130)	(1.2)	(5.146)	(130)	(1.2)
axial ratio (a/b)						
100	5.245	5.245	0.461	5.159	5.271	0.552
10	5.241	5.242	0.465	5.160	5.266	0.550
5	5.234	5.239	0.471	5.162	5.258	0.547
2	5.209	5.229	0.493	5.166	5.234	0.539
1	5.169	5.23	0.534	5.169	5.230	0.535
0.1				5.133	5.989	0.625
	Amorphous Ellipsoids in a Crystalline Matrix					
exptl results	(5.146)	(130)	(1.2)	(5.146)	(130)	(1.2)
axial ratio (a/b)						
10	5.23	977.45	6.556	5.095	354.17	3.902
5	5.22	356.66	3.963	5.094	148.26	2.534
2	5.16	115.88	2.258	5.092	72.0	1.777
1	5.09	61.58	1.647	5.091	61.52	1.646
0.1				5.1	216.85	2.815

Table VI
Relaxation Parameters of Sample H34A Predicted by MWS Theory

	parallel			random		
	ϵ_∞	ϵ_s	$\bar{\tau}_D$	ϵ_∞	ϵ_s	$\bar{\tau}_D$
	Crystalline Ellipsoids in an Amorphous Matrix					
exptl results	(4.777)	(105)	(3.35)	(4.777)	(105)	(3.35)
axial ratio (a/b)						
100	4.896	4.896	1.10	4.793	4.937	1.3
10	4.891	4.893	1.11	4.794	4.931	1.3
5	4.883	4.889	1.12	4.796	4.921	1.29
2	4.852	4.880	1.17	4.801	4.898	1.27
1	4.804	4.886	1.26	4.804	4.886	1.26
0.1				4.767	5.566	1.42
	Amorphous Ellipsoids in a Crystalline Matrix					
exptl results	(4.777)	(105)	(3.35)	(4.777)	(105)	(3.35)
axial ratio (a/b)						
10	4.88	653.07	13.50	4.723	237.1	8.02
5	4.86	238.75	8.16	4.722	99.67	5.21
2	4.80	78.05	4.66	4.719	48.77	3.67
1	4.77	41.81	3.40	4.718	41.77	3.40
0.1				4.731	133.79	6.04

Table VII
Relaxation Parameters of Sample H49A Predicted by MWS Theory

	parallel			random		
	ϵ_∞	ϵ_s	$\bar{\tau}_D$	ϵ_∞	ϵ_s	$\bar{\tau}_D$
	Crystalline Ellipsoids in an Amorphous Matrix					
exptl results	(4.277)	(52)	(11.2)	(4.277)	(52)	(11.2)
axial ratio (a/b)						
100	4.425	4.425	3.576	4.299	4.480	4.128
10	4.419	4.423	3.597	4.300	4.473	4.120
5	4.408	4.418	3.640	4.302	4.463	4.105
2	4.370	4.410	3.793	4.307	4.436	4.069
1	4.310	4.423	4.047	4.310	4.423	4.050
0.1				4.274	4.952	4.317
	Amorphous Ellipsoids in a Crystalline Matrix					
exptl results	(4.277)	(52)	(11.2)	(4.277)	(52)	(11.2)
axial ratio (a/b)						
10	4.41	369.237	36.595	4.223	134.65	21.638
5	4.39	135.583	22.138	4.221	57.15	14.110
2	4.31	44.956	12.655	4.217	28.44	9.972
1	4.22	24.517	9.268	4.215	24.49	9.260
0.1				4.236	76.39	16.334

persed in an interconnected crystalline matrix. The axial ratio of the amorphous ellipsoids thus predicted is approximately 1 for both samples of H34 and about 5 for samples H49A and H63A. These predictions are consistent with earlier studies of morphology in the same sample system.[9] It has been shown that a compression-molded sample of H34 has a nonspherulitic but interconnected crystalline structure, while both samples H49 and H63 are spherulitic. An idealized model of a space-filling spherulitic structure is illustrated in Figure 15 (four spherulites shown). The ribbon-like crystalline lamellae radiate from the nucleus of the spherulite with substantial branching.

Table VIII
Relaxation Parameters of Sample H63A Predicted by MWS Theory

	parallel			random		
	ϵ_∞	ϵ_s	$\bar{\tau}_D$	ϵ_∞	ϵ_s	$\bar{\tau}_D$
	Crystalline Ellipsoids in an Amorphous Matrix					
exptl results	(4.046)	(50)	(18.62)	(4.046)	(50)	(18.62)
axial ratio (a/b)						
100	4.226	4.226	7.06	4.076	4.264	7.94
10	4.219	4.223	7.09	4.077	4.258	7.93
5	4.206	4.218	7.17	4.079	4.248	7.91
2	4.159	4.205	7.43	4.085	4.224	7.87
1	4.088	4.212	7.84	4.088	4.212	7.84
0.1				4.051	4.592	8.13
	Amorphous Ellipsoids in a Crystalline Matrix					
exptl results	(4.046)	(50)	(18.62)	(4.046)	(50)	(18.62)
axial ratio (a/b)						
10	4.21	250.578	63.92	3.988	91.82	37.64
5	4.18	92.451	38.67	3.985	39.37	24.61
2	4.09	31.119	22.16	3.979	19.94	17.47
1	3.98	17.287	16.26	3.976	17.27	16.25
0.1				4.007	52.39	28.48

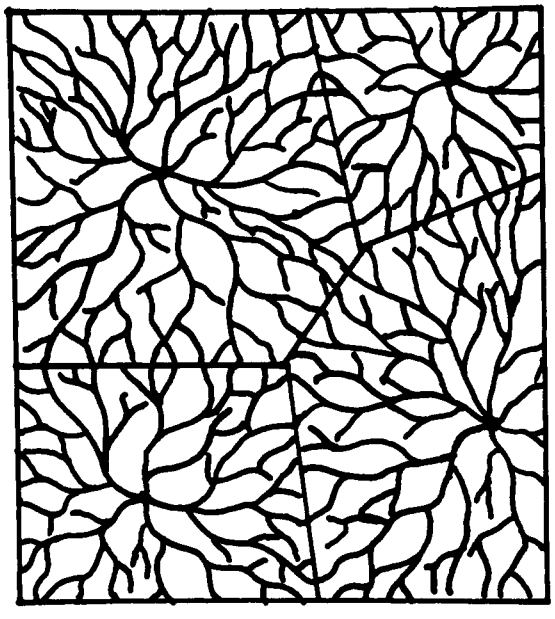

Figure 15. Schematic model of spherulites.

The interlamellar amorphous phase is suggested to be capable of approximation by ellipsoids, although in a real system they may not be completely discontinuous. The random nature of the ellipsoids directly results from the unoriented spherulitic structure.

Conclusions

Dielectric relaxation studies of segmented polyesters reveal several relaxation processes which occur over a broad range of the temperature–frequency domain. The γ relaxation occurring at low temperatures (high frequency) involves local mode motion of the noncrystalline phase containing polyether segments as well as the C=O groups of the hard segments. The effect of the latter group on this process is diminished in samples containing 63 wt % or less of the 4GT segments. At higher temperatures, the β relaxation involves micro-Brownian motion of the amorphous phase, which consists of partially mixed polyether segments and uncrystallized 4GT segments. The activation energy of this process varies as a function of composition from that of the activation energy of the T_g process for the PTMO homopolymer to that of pure PTMT. Samples treated by annealing and absorption of water exhibit a lower T_g than do the control samples. The annealed sample shows a decrease in the activation energy of the T_g process, while an increase in activation energy for the wet sample has been observed. Above T_g, the α relaxation process is associated with defects in the 4GT crystalline phase. Finally, at very low frequencies or at high temperatures, interfacial polarization occurs at the crystalline–amorphous boundaries.

A newly designed ULF dielectric measuring system has been described which requires no time-consuming balancing and calibration procedure. Computation of the unknown R_x and C_x of the sample is relatively simple. Since there is no transient term involved in the course of measurements, the technique can practically and conveniently cover the frequency range of 10 to 10^{-4} Hz.

The two-phase structure of these segmented copolymers was studied by analysis of low-frequency dielectric spectra, which show the Maxwell–Wagner–Sillars interfacial polarization. The experimental results can be modeled by MWS dielectric theory, which suggests that the crystalline phase is interconnected about an occluded amorphous phase of randomly oriented amorphous spheroids.

Acknowledgment. The authors wish to thank Dr. G. M. Estes of E. I. DuPont de Nemours and Co. for supplying the segmented copolyester studies. This work has been supported by the National Science Foundation Polymer Materials Program through Grant No. DMR 78-11662.

References and Notes

(1) M. Brown and W. K. Witsieppe, *Rubber Age (N.Y.)*, **104** (3), 35 (1972).
(2) W. K. Witsieppe, *Adv. Chem. Ser.*, **129**, 39 (1973).
(3) G. K. Hoeschele and W. K. Witsieppe, *Agnew. Makromol. Chem.*, **29/30**, 267 (1973).
(4) R. J. Cella, *J. Polym. Sci., Polym. Symp.*, **42**, 727 (1973).
(5) W. H. Buck, R. J. Cella, E. K. Gladding, and J. R. Wolfe, *J. Polym. Sci., Polym. Symp.*, **48**, 47 (1974).
(6) G. K. Hoeschele, *Polym. Eng. Sci.*, **14**, 848 (1974).
(7) M. Shen, U. Mehra, M. Niinomi, J. K. Koberstein, and S. L. Cooper, *J. Appl. Phys.*, **45** (10), 4182 (1974).
(8) R. W. Seymour, J. R. Overton, and L. S. Corley, *Macromolecules*, **8**, 331 (1975).
(9) A. Lilaonitkul, J. C. West, and S. L. Cooper, *J. Macromol. Sci. Phys.*, **12** (4), 563 (1976).
(10) A. Lilaonitkul and S. L. Cooper, *Rubber Chem. Technol.*, **50**, 1 (1977).
(11) J. W. C. Van Bogart, A. Lilaonitkul, L. E. Lerner, and S. L. Cooper, *J. Macromol. Sci. Phys.*, accepted for publication.
(12) A. M. North, R. A. Pethrick, and A. D. Wilson, *Polymer*, **19**, 913 (1978).
(13) A. M. North, R. A. Pethrick, and A. D. Wilson, *Polymer*, **19**, 923 (1978).

(14) N. G. McCrum, B. Read, and G. Williams, "Anelastic and Dielectric Effects in Polymer Solids", Wiley, New York, 1967.
(15) M. E. Baird, "Electrical Properties of Polymeric Materials", The Plastics Institute, London, 1973.
(16) R. W. Sillars, *J. Inst. Elec. Eng.*, **80**, 378 (1937).
(17) L. K. H. Van Beek, *Prog. Dielectr.*, **7**, 69 (1967).
(18) M. E. Baird, *Rev. Mod. Phys.*, **40**, 219 (1968).
(19) S. B. Dev, A. M. North, and J. C. Reid in "Dielectric Properties of Polymers", F. E. Karaz, Ed., Plenum Press, New York, 1972.
(20) W. P. Harris, *Annu. Rep. Conf. Electr. Insul. Dielectr. Phenom.*, **No. 1481**, 72 (1967).
(21) S. Robert, Report No. 66-0-333, General Electric R&D Center, Schenectady, N.Y., 1966.
(22) J. G. Berberian and R. H. Cole, *Rev. Sci. Instrum.*, **40** (6), 811 (1969).
(23) R. S. Lakes and R. A. Harper, *Rev. Sci. Instrum.*, **46** (11), 1583 (1975).
(24) M. Gordon and J. S. Taylor, *J. Appl. Chem.*, **2**, 493 (1952).
(25) I. Kirshenbaum, *J. Polym. Sci., Part A*, **3**, 1869 (1965).
(26) U. Alter and R. Bonart, *Colloid Polym. Sci.*, **254**, 348 (1976).
(27) F. P. Warner, D. S. Brown, and R. E. Wetton, *J. Chem. Soc., Faraday Trans. 2*, **72**, 1064 (1976).
(28) I. H. Hall and M. G. Pass, *Polymer*, **17**, 807 (1976).
(29) C. R. Ashcraft and R. H. Boyd, *J. Polym. Sci., Part A-2*, **14**, 2153 (1976).
(30) R. E. Wetton and G. Williams, *Trans. Faraday Soc.*, **61**, 2132 (1965).
(31) R. E. Wetton, G. S. Fielding-Russell, and K. U. Fulcher, *J. Polym. Sci., Part C*, **30**, 219 (1970).
(32) S. de Petris, V. Frosini, and E. A. Nicol, *J. Polym. Sci., Part A-2*, **15**, 1121 (1977).
(33) F. Stern and C. Weaver, *J. Phys. C*, **3**, 1736 (1970).
(34) J. R. Macdonald, *J. Chem. Phys.*, **54**, 2026 (1971).
(35) C. T. O'Konski, *J. Phys. Chem.*, **64**, 605 (1960).
(36) H. Looyenga, *Physica (Utrecht)*, **31**, 401 (1965).
(37) W. E. A. Davies, *Br. J. Appl. Phys.*, **7**, 120 (1974).

Conformational Energy Minimization in the Approximation of Limited Range Interactions

Robert L. Jernigan* and Shousun C. Szu‡

Laboratory of Theoretical Biology, National Cancer Institute, National Institutes of Health, Bethesda, Maryland 20205. *Received March 19, 1979*

ABSTRACT: A general method to determine the conformational free energy minimum is developed by approximating the total molecular free energy as the sum of contributions from independent segments, each of which can exist in several conformations. The simple algorithm to determine the best overall conformation rigorously yields the same results as those obtained by enumerating all possible combinations of independent segments. However, the method, based upon dynamic programming concepts, is much simpler because it avoids explicit generation of all possible combinations of segments. Application of the method to protein secondary structures is discussed. Development of this conformational selection scheme is independent of the method by which free energies have been calculated. An example is presented for determining relative preferences for α-helix and β-strand in a fragment of trypsin inhibitor.

The simplest considerations based on small molecules would lead to the postulation of myriad forms for large molecules; however, frequently a unique conformation is observed for many large biological macromolecules. Determining such preferred conformations for proteins has been attempted by traversing conformational space to determine the conformations of lowest free energy.[1] An exhaustive search of conformational space is usually impossible for all except the smallest molecules; therefore, the existence of numerous local minima renders the detection of a global minimum particularly difficult. Here we are attempting to approximate molecular free energies and to shorten the list of conformations in order to simplify the search for minima.

Energies are approximated by including only interactions within molecular segments. The total molecular energy is approximated as the sum of segment energies; the assumption is that the intrasegment interactions will include the majority of all molecular interactions. Application of a concept from dynamic programming permits a shortening of the number of combinations of segments which must be considered.

Method

The method presented below is a practical approach to this problem. Interatomic interactions here are to be limited to those within single regularly structured regions. All possible regions are considered; the combination of such regions with the lowest total free energy is determined. Because of the compact nature of globular proteins, an individual regular region usually includes only a small fraction of the atoms in the whole molecule. A regular region in a protein is taken to be one in which the backbone rotation angles are identical, within some permitted range of variation. Interatomic interactions which can be included here are all those within each such region, of both short and medium range.

Consider a linear molecule of N residues, each of which can exist in one of ζ regular conformational states. For this approach, it is necessary to specify k, the maximum length of such regions. This will correspond to the maximum range of interactions to be included. Further, it is assumed here that there are no interactions between separate regular regions; such interactions could be included by a simple modification of the method. In the present version of this method, it is important that the regions be relatively long, so as to include, on the average, the majority of interatomic interactions.

The free energy of a region encompassing residues $i-j$ through i is given as $F^{\xi_{i-j}\xi_{i-j+1}\cdots\xi_i}_{i-j,i}$, where the conformational states of each residue included in the region are specified by the ξ's. The present method requires that a complete set of such free energies can be calculated and is available. Calculation of these energies must involve approximations; that is the subject of other work.[2]

The formalism of the selection process is necessarily directional. The choice of a direction in which to proceed is, however, arbitrary; with independent regions, the results are independent of this direction. Here we proceed from

‡ Division of Bacterial Products, Bureau of Biologics, Food and Drug Administration, Bethesda, Maryland 20205.